Temperature dependence of vesicle adhesion

Thomas Gruhn and Reinhard Lipowsky
Max-Planck-Institut für Kolloid- und Grenzflächenforschung, 14424 Potsdam, Germany
(Received 2 September 2004; published 12 January 2005)

The influence of thermal fluctuations on the adhesion behavior of fluid vesicles is investigated with the help of Monte Carlo simulations. The adhesion area A_{ad} of a fluid vesicle adhering to a smooth attractive substrate is studied systematically for different values of temperature, adhesion strength, and potential range. For low temperatures T, the ratio A_{ad}/A between the adhesion area and the total area A of the vesicle is a linear function of T/κ, where κ is the bending rigidity. Linear fits of the simulation data allow an extrapolation to $T=0$ which corresponds well with data obtained from a simplified analytic model. A new ansatz for $A_{ad}(T)$ which is based on the eigenmodes of the adhering vesicle explains the linear behavior of $A_{ad}(T)$ for low T and helps to define a fit function which reproduces the linear behavior of the obtained simulation data. This fit function may be used in order to determine the bending rigidity and the adhesion strength from the observed adhesion geometry.

DOI: 10.1103/PhysRevE.71.011903 PACS number(s): 87.16.Dg, 87.16.Ac, 68.15.+e

I. INTRODUCTION

The adhesion of cells to solid materials or to other cells is essential for the existence of multicellular life forms. The principles of cell adhesion are not only a fundamental aspect of cell biophysics, it is also of biotechnological relevance for the development and improvement of interfaces between living cells and artificial materials. Typical applications are the development of biosensors [1,2] and the creation of improved implantation materials [3,4].

The adhesion behavior of cells depends strongly on the mechanical and chemical properties of the flexible membrane shell that surrounds the cell interior. The cell membrane consists predominantly of a lipid bilayer. Fluid vesicles are hollow lipid bilayer shells. In the lab they serve as biomimetic model systems for the study of cell properties which do not strongly depend on the cell interior. An overview of the large number of experimental and theoretical studies of vesicles can be found in [5,6]. The shape of adhering vesicles has been investigated experimentally using various techniques including reflection interference contrast microscopy [7,8], fluorescence microscopy [9,10], atomic force microscopy [11], and freeze-fracture electron microscopy [12,13].

Lipid membranes have a thickness of about 4–5 nm, while giant vesicles can have a diameter of 10 μm and larger. Therefore, on sufficiently large scales, the membrane behaves as a two-dimensional surface. The shape of the vesicle depends on the external conditions and the membrane's material properties that determine the elastic energy of the vesicle. The most relevant elastic properties are the bending rigidity κ and the spontaneous curvature M_{sp}. In general, the spontaneous curvature of a membrane bounding a closed vesicle will have both local contributions arising from the bilayer asymmetry or from the asymmetry of the surrounding aqueous solution and global contributions arising from the vesicle closure; the latter contribution has been systematically studied in Ref. [14]. In the following, we will assume that the total spontaneous curvature, which contains all of these different contributions, is small and, thus, will focus on the case of zero spontaneous curvature. Then, the vesicle shape is governed by the interplay of external constraints and the elastic curvature energy proportional to κ. The value of κ typically depends on the membrane material and the temperature. For unbound vesicles, the bending rigidity can be measured by analyzing its fluctuation spectrum [15,16].

If a vesicle adheres to a planar substrate, its morphology also depends on the properties of the adhesion potential. In the absence of thermally excited fluctuations, the shape of an adhering vesicle has been calculated in detail using free-energy functional minimization techniques [17–19]. Much less is known about the morphology of vesicles at finite temperature.

With the help of Monte Carlo simulations, we study systematically the temperature dependence of the adhesion behavior. Simulations are performed at several temperatures and for various adhesion potentials. It is found that for a broad parameter range, the adhesion area can be related to the temperature, the adhesion strength, and the bending rigidity by a simple formula. In cases where the temperature dependence of the vesicle surface size and of κ are small or approximately known, the formula can be used in the experiment to determine the adhesion strength and the bending rigidity of the vesicle from measurements of the adhesion area.

The outline of this article is as follows. The theoretical models for vesicle adhesion are specified in Sec. II, and the simulation method is explained in Sec. III. In Sec. IV, results of the simulations are presented and extrapolated towards $T=0$. A simplified model is introduced in Sec. V which allows an analytic study of adhering vesicles at $T=0$. Results from the simplified model are analyzed and compared with the simulation results. In Sec. VI, the temperature dependence of vesicle adhesion is analyzed, and a new analytic framework for adhesion at finite temperature is presented. Finally, the application of the obtained results for adhesion experiments is discussed in Sec. VII, before some final conclusions are made in Sec. VIII. In Appendix A, the energy terms of the simplified model in Sec. V are derived.

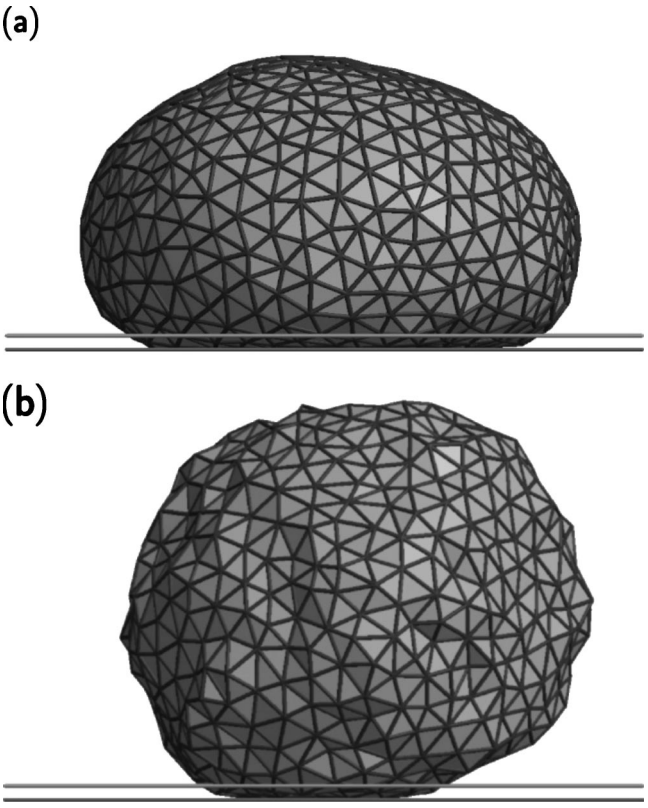

FIG. 1. Snapshots of a vesicle adhering to a substrate potential of range $\hat{d}=0.06$ and adhesion strength $w=6.3$ at temperatures (a) $\hat{T}=0.025$ and (b) $\hat{T}=0.25$. The horizontal lines indicate the range of the substrate potential.

II. THEORETICAL MODEL

The vesicle membrane is modeled as a two-dimensional homogeneous surface S_{ves} with area A. The vesicle is in contact with a smooth planar substrate (Fig. 1). The adhesion is caused by an attractive short-range potential of the substrate which is represented by a square-well potential with range d. The adhesion (free) energy is then given by

$$E_{ad} = \int_{S_{ves}} dAV(z) \tag{2.1}$$

with

$$\begin{aligned} V(z) &= \infty, \quad z < 0, \\ &= -W, \quad 0 \leqslant z < d, \\ &= 0, \quad d \leqslant z, \end{aligned} \tag{2.2}$$

where $W>0$ is the adhesion energy per attached membrane area and z denotes the distance between the surface element and the wall plane. The square-well potential determines the adhesion zone of the membrane unambiguously: The adhesion zone S_{ad} consists of all regions of S_{ves} which are closer to the substrate than the potential range d. The (intrinsic) adhesion area is given by

$$A_{ad} = \int_{S_{ad}} dA. \tag{2.3}$$

In general, a pressure difference ΔP may exist between the fluid regions inside and outside the vesicle membrane so that small changes dV of the vesicle volume are connected with the work $\Delta P(V)dV$. Such pressure differences are induced by molecules in and outside the vesicle whose permeation rate through the membrane is low or zero. In this article, we consider the case that the concentration of such molecules is small so that $\Delta P=0$. Furthermore, zero spontaneous curvature $M_{sp}=0$ of the vesicle's membrane is considered. The elastic curvature energy of one configuration can then be expressed as [20]

$$E_{el} = \frac{\kappa}{2} \int_{S_{ves}} dA(2M)^2, \tag{2.4}$$

where M is the local mean curvature.

A plausible model scenario for vesicle adhesion consists of a vesicle in a half-space with a substrate at $z=0$ which has a suitably strong, attractive short-range potential. However, from a strict point of view at thermal equilibrium, the vesicle is never bound in such a system: If z_0 denotes the smallest distance between the vesicle and the substrate, the vesicle is bound for all states with $0 \leqslant z_0 < d$, while it is unbound for $d \leqslant z_0 < \infty$, an infinitely large interval. Thus, at a finite temperature the vesicle is, on average, always unbound, no matter how deep and broad the adhesion potential is. The situation in the lab is, however, different: Typically, the vesicle can only be a distance $z_{\max} < 10$ mm away from the substrate before it contacts another surface. The partition function of a vesicle with $0 \leqslant z_0 \leqslant z_{\max}$ can be divided into bound and unbound states,

$$\begin{aligned} Z &= Z_{bound} + Z_{unbound} \\ &\equiv \int_0^d dz_0 \int_{shapes} \int_{S_{ves}} dA e^{-(E_{ad}+E_{el})/T} \\ &\quad + \int_d^{z_{max}} dz_0 \int_{shapes} \int_{S_{ves}} dA e^{-E_{el}/T} \\ &\simeq [e^{-\langle E_{ad}\rangle/T} d + (z_{max} - d)] \int_{shapes} \int_{S_{ves}} e^{-E_{el}/T}. \end{aligned} \tag{2.5}$$

Here, $\int_{shapes}$ includes all vesicle configurations with wall distance z_0. The temperature T is expressed in energy units so that the Boltzmann factor is contained in T. Since $z_{max} \gg d$, one gets

$$Z_{bound}/Z_{unbound} \simeq \frac{\exp(-\langle E_{ad}\rangle/T)}{z_{max}/d}. \tag{2.6}$$

The simulations in this article are restricted to bound states. This is justified if

$$|\langle E_{ad}\rangle/T| > \ln(z_{max}/d) \simeq 16. \tag{2.7}$$

In the following, the bending rigidity κ is taken to provide the basic energy scale. The notation $\hat{E} \equiv E/\kappa$ is used for dimensionless energy quantities. The total membrane area A defines the length scale $R \equiv \sqrt{A/(4\pi)}$ which is characteristic for the vesicle's linear dimensions. It should be mentioned that our investigations are not restricted to the case of temperature-independent κ and R. The consequences of such such temperature dependences are discussed in Sec. VII. The described model system, which mimics a vesicle in contact with a smooth, planar attractive substrate, depends on three parameters: The reduced temperature $\hat{T}$, the reduced potential depth w, and the reduced potential range $\hat{d}$, defined as

$$\hat{T} \equiv T/\kappa, \tag{2.8}$$

$$w \equiv WR^2/\kappa, \tag{2.9}$$

$$\hat{d} \equiv d/R. \tag{2.10}$$

III. SIMULATION METHOD

On length scales which are large compared to the size of the lipid molecules, the vesicle membrane can be taken to be a smooth, deformable surface. In the Monte Carlo simulations, the shape of the vesicle is discretized using a flexible polyhedron of N_t triangles. The triangles are bounded by edges $\underline{c}_n$ with $n=1,\ldots,N_e$ which interconnect the vertices of the triangulated vesicle. A configuration of the triangulated vesicle is fully determined by the locations $\underline{r}_i$ of the $N_v = N_t/2+2$ vertices and a table of the pairs of vertices that are connected by one of the edges. During the simulation, the tethered bead model [21] is applied, which corresponds to the energy expression

$$\begin{aligned} \hat{E}_b = \infty \quad & \|\underline{r}_j - \underline{r}_i\| < \ell \quad (\text{for any } i \neq j = 1, \ldots, N_v), \\ = \infty \quad & \|\underline{r}_j - \underline{r}_i\| > \ell + \Delta\ell \quad (\text{for any } \underline{r}_i, \underline{r}_j \text{ connected}), \\ = 0 \quad & \text{otherwise} \end{aligned} \tag{3.1}$$

so that the distance between two connected vertices is restricted to $\ell < \|\underline{r}_i - \underline{r}_j\| < \ell + \Delta\ell$, where $\Delta\ell = 0.7\ell$. An additional constraint restricts the fluctuations of the membrane's total area A_{sim} to $|A_{sim} - A| < 0.025A$.

The elastic curvature energy of the vesicle is discretized according to [22]

$$\hat{E}_{el} = 2\sum_{J=1}^{N_t} (M\Delta A)_J^2/\Delta A_J, \tag{3.2}$$

where ΔA_J is the area of triangle J and $(M\Delta A)_J$ is the contribution of triangle J to the total mean curvature of the vesicle. It is defined as

$$(M\Delta A)_J = \frac{1}{4}\sum_K{}' \|\underline{r}_j - \underline{r}_k\| \arccos(\underline{e}_J \cdot \underline{e}_K), \tag{3.3}$$

where the sum goes over the neighbor triangles K. The vectors $\underline{r}_j$ and $\underline{r}_k$ point to the two vertices that are shared by triangle J and K. The unit vectors $\underline{e}_J$ and $\underline{e}_K$ are normals of triangle J and K, respectively, and point to the outside of the vesicle.

The reduced adhesion energy is given by

$$\hat{E}_{ad} = -wA_{ad}/R^2. \tag{3.4}$$

In the simulations, the vesicle is represented by a network of $N_t = 1280$ triangles. Each Monte Carlo sweep consists of N_v attempts to move a vertex, one attempt to move the whole vesicle, one attempt to rotate the vesicle, and $3N_v$ attempts to flip an edge. The edge flip proceeds as follows: Each edge lies between two triangles. Together, the two triangles have four vertices, two of which are connected by the shared edge. In an edge flip, the shared edge is moved such that it connects the formerly unconnected vertices. Typically 1.5×10^6 Monte Carlo sweeps were performed for each choice of parameters. Half of the sweeps were used to ensure complete equilibration of the system.

IV. RESULTS

For sufficiently small $\hat{T}$, vesicles are bound so that the relative adhesion area

$$\alpha \equiv A_{ad}/A \tag{4.1}$$

is larger than zero. In the limit of vanishing $\hat{T}$, the relaxation time diverges and inhibits efficient simulations. Above a certain temperature $\hat{T}_{ub}$, the vesicle unbinds and α vanishes. Between these extrema, the behavior of $\alpha(\hat{T})$ is analyzed with the help of Monte Carlo simulations, which are performed for various choices of the wall potential. Potential ranges $\hat{d} = 0.03$, 0.06, and 0.09 are considered. Values for the reduced potential depth w are chosen between $w = 2.8$ and $w = 25$. For each set of w and $\hat{d}$, the temperature is varied between $0.025 \leqslant \hat{T} \leqslant 0.25$ corresponding to bending rigidities from $\kappa = 40T$ down to $\kappa = 4T$. Figure 2(a) shows results of $\alpha(\hat{T})$ for the potential depth $\hat{d} = 0.09$. For all chosen values of w the results of $\alpha(\hat{T})$ can be fitted very well by a linear function of $\hat{T}$. The slope of $\alpha(\hat{T})$ is weakly dependent on w; the rate $-d\alpha/d\hat{T}$ at which the adhesion area shrinks decreases with increasing w. As shown in Fig. 2(b), a linear behavior of $\alpha(\hat{T})$ is also found for $\hat{d} = 0.06$, as long as $\hat{T}$ is small. For $\hat{T} > 0.15$, the data points of α decrease faster than linearly with increasing $\hat{T}$. Results for $\hat{d} = 0.03$ are shown in Fig. 2(c). The behavior of $\alpha(\hat{T})$ is similar to that for $\hat{d} = 0.06$ but the linear regime is limited to even smaller values of $\hat{T}$, especially for small w.

The linear behavior of $\alpha(\hat{T})$ at low $\hat{T}$ allows a simple extrapolation towards $\hat{T} = 0$. The values of $\alpha(\hat{T} = 0)$ which are used in the following are obtained from a linear extrapolation of the data points at $\hat{T} = 0.025 - 0.075$; a quadratic fit of the results for $\hat{T} = 0.025 - 0.1$ produces almost the same results. The straight lines in Fig. 2 represent the fit functions. The

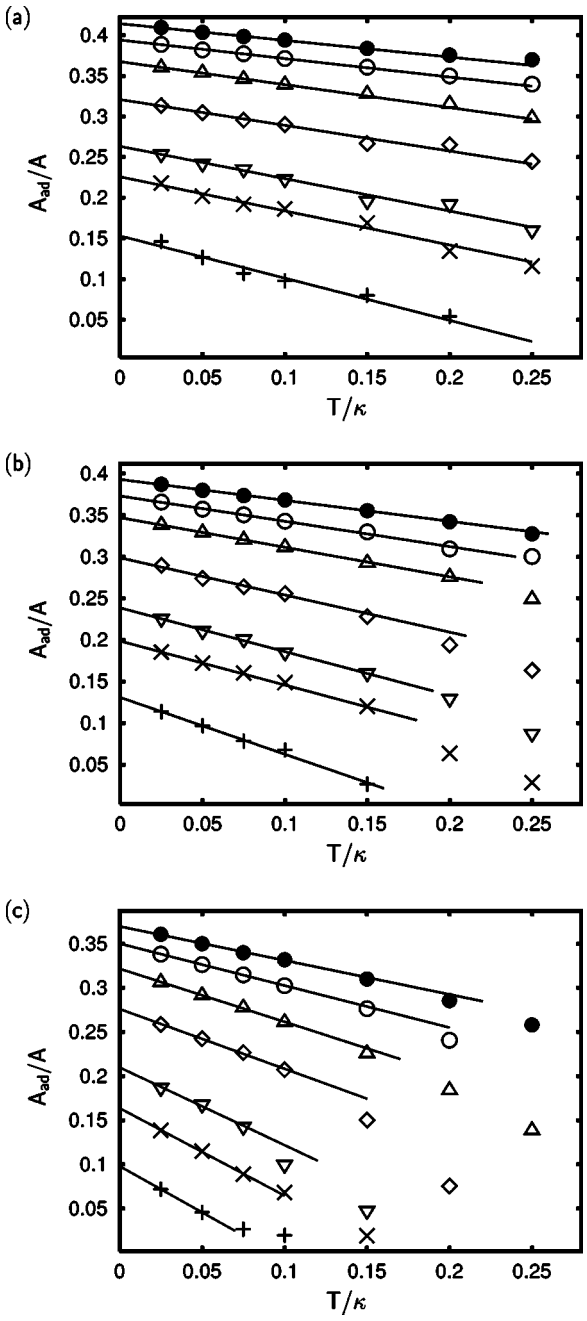

FIG. 2. The relative adhesion area A_{ad}/A as a function of $\hat{T}$ for potential ranges (a) $\hat{d}=0.09$, (b) $\hat{d}=0.06$, (c) $\hat{d}=0.03$. The data points are simulation results for $w=2.8$ (+), $w=4.8$ (×), $w=6.3$ (▽), $w=10.0$ (◇), $w=15.0$ (△), $w=20.0$ (○), and $w=25.0$ (●). The straight lines are linear fits of the low-temperature regions.

corresponding values obtained for $\alpha(\hat{T}=0;w)$ are plotted in Fig. 3 as a function of w. In order to discuss these results and check the accuracy, a simplified model of an adhering vesicle is introduced in the next section which allows an analytic treatment of such vesicles at $\hat{T}=0$.

V. CAPLIKE SHAPES AT ZERO TEMPERATURE

We introduce a simplified analytical model for an adhering vesicle. The deformations of this vesicle are restricted to

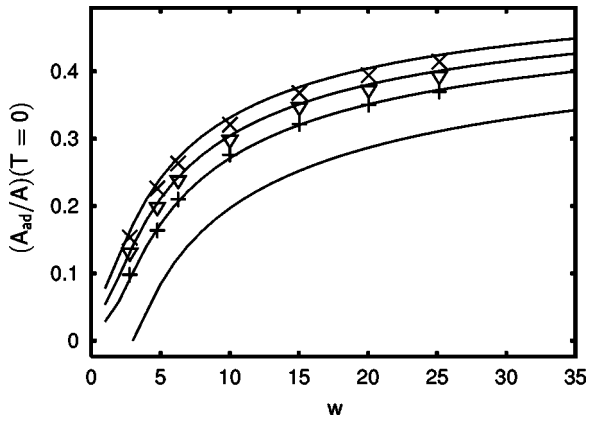

FIG. 3. The relative adhesion area A_{ad}/A at $T=0$ as a function of w. The symbols denote extrapolations from the simulation results for $\hat{d}=0.03$ (+), $\hat{d}=0.06$ (▽), and $\hat{d}=0.09$ (×). The curves show solutions from the simple model described in Sec. V. Solutions are given for $\hat{d}=0$, $\hat{d}=0.03$, $\hat{d}=0.06$, and $\hat{d}=0.09$ from the lowest to the highest curve.

a set of shapes for which the configurational energy can be obtained analytically.

For $\hat{T}\ll 1$, $\hat{d}\ll 1$, and sufficiently large w, the equilibrium shape of an adhering vesicle is known to consist of a circular disklike area on the substrate, a spherical cap on the opposite side, and a small intermediate region of strong curvature along the contact line [19]. Configurations for smaller values of w are approximately of the same shape; only the region between the flat and the spherical cap gets broader. Therefore, we take the shape of the adhering vesicle to consist of a spherical cap with radius R_{sc}, a circular base area of radius R_{ba}, and a *torus segment* that connects the other two. The connecting torus segment has a small curvature radius R_{co} and a large curvature radius R_{ba}, as shown in the sketch in Fig. 4. The small curvature radius R_{co} is set to

$$R_{co} \equiv \frac{R}{\sqrt{2w}}, \tag{5.1}$$

which is the equilibrium contact curvature of adhering vesicles at $T=0$ [17].

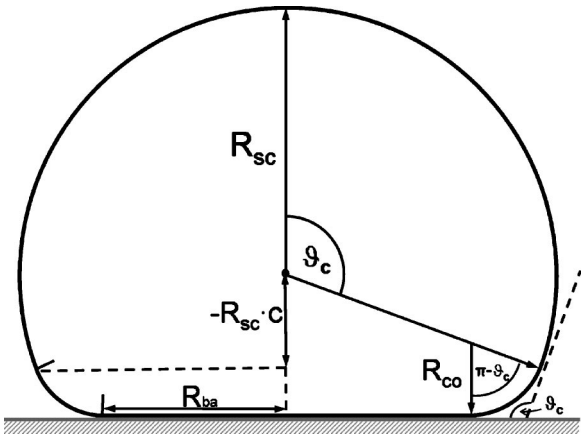

FIG. 4. Geometry of the simplified model.

In the simplified model, the shape of the vesicle is controlled by the parameter

$$c \equiv \cos(\theta_c), \tag{5.2}$$

where θ_c is the effective contact angle of the adhering vesicle [17]. The total height of the vesicle is equal to $R_{sc}(1-c)+R_{co}(1+c)$.

The energy E of the model vesicle is determined by c, $\hat{d}$, and w. In Appendix A, an analytic expression is derived for $E=E_{ad}+E_{el}$, which is composed of the adhesion energy $E_{ad}=-WA_{ad}$ and the elastic curvature energy E_{el}.

For a contact potential with $\hat{d}=0$, the adhesion area A_{ad} coincides with the base area A_{ba}. For $\hat{d}>0$, also parts of the torus region contribute to A_{ad}; if $\hat{d}>(1+c)/\sqrt{2w}$, the adhesion area includes the full torus segment and a part of the sphere cap. In terms of the two parameters

$$m \equiv \min\{\hat{d}\sqrt{2w}, 1+c\} \tag{5.3}$$

and

$$\lambda \equiv R_{ba}/R_{co}, \tag{5.4}$$

the adhesion energy can be expressed as

$$E_{ad} = -\pi\kappa\left[\frac{1}{2}\lambda^2 + \lambda \arccos(1-m) + m + \left(\frac{\lambda}{\sqrt{1-c^2}}+1\right)(\hat{d}\sqrt{2w}-m)\right]. \tag{5.5}$$

For $\lambda \neq 1$, the elastic curvature energy has the form

$$E_{el} = 2\pi\kappa\left[4 + \frac{\lambda^2}{\sqrt{\lambda^2-1}}\arctan\left(\frac{(1+c)\sqrt{\lambda^2-1}}{(1+c)+\lambda\sqrt{1-c^2}}\right)\right]. \tag{5.6}$$

The behavior of E_{el} is further discussed in Appendix A, see Eq. (A16), where the case $\lambda=1$ is considered as well, and complex numbers are avoided for $\lambda<1$.

For given values of w and $\hat{d}$, the equilibrium configuration of the model system at $\hat{T}=0$ is determined by the value $c=c_{min}$ for which $E(w,\hat{d};c)$ is minimum. In Fig. 3, the resulting reduced adhesion areas $\alpha=A_{ad}/A$ at $\hat{T}=0$ are shown for $\hat{d}=0.03$, 0.06, and 0.09 together with the extrapolations from the simulations. The extrapolated simulation results are slightly lower than the model predictions but the agreement is quite remarkable, especially since no fit parameter has been used.

If the adhesion strength w is smaller than a threshold value w_{thr}, the vesicle is perfectly spherical. For $w \geqslant w_{thr}$, an energy minimum exists at a value $c_{min} \geqslant -1$ for which $dE/dc(w,\hat{d};c_{min})=0$. At the threshold adhesion strength w_{thr}, one has $c_{min}=-1$ so that $dE/dc(w_{thr},\hat{d};c=-1)=0$.

We consider a finite potential range $\hat{d}>0$, a finite w, and a value for the contact angle parameter c which is so close to -1 that it satisfies the inequality $c+1<\hat{d}\sqrt{2w}$. Then, in Eq. (5.5) one has $m=c+1$ and the derivative of E with respect to c becomes

$$\frac{dE}{dc} = -\pi\kappa(1-\sqrt{2w})^2\left[1-(1-\sqrt{2w})^{-1}+2\ln\left(1-\frac{1}{\sqrt{2w}}\right)\right] + O(c+1). \tag{5.7}$$

For $c=-1$, the only solution of $dE/dc=0$ is

$$w_{thr} = 1/2 \ (\hat{d}>0), \tag{5.8}$$

which turns out to be independent of the choice of $\hat{d}>0$. The slope of $\alpha(w)$ at w_{thr} is

$$\frac{d\alpha}{dw}(w_{thr}) = \frac{3}{8}\left(1-\frac{\hat{d}}{4}\right) \ (\hat{d}>0). \tag{5.9}$$

For $0<w<1/2$, the vesicle configuration with the lowest energy is a perfect sphere with a relative adhesion area $\alpha=\hat{d}/2$ so that the total energy is given by $E_{sph}\equiv 8\pi\kappa-2\pi\kappa w\hat{d}$.

On the other hand, for a contact potential with $\hat{d}=0$ one has $m=0$ in Eq. (5.5) and

$$\frac{dE}{dc} = -\pi\kappa(1-\sqrt{2w})^2\left[1+2\ln\left(1-\frac{1}{\sqrt{2w}}\right)\right] + O(c+1) \tag{5.10}$$

for $c \simeq -1$. Here, $E(w,0;c=-1)$ is maximum at $w=1/2$, while it is minimum at

$$w_{thr} = \frac{e}{2(1-\sqrt{e})^2} \simeq 3.23 \ (\hat{d}=0). \tag{5.11}$$

For this adhesion strength, the adhesion area vanishes and the vesicle unbinds. The slope

$$\frac{d\alpha}{dw}(w_{thr}) = \frac{\sqrt{e}-1}{8w_{thr}^2(\sqrt{e}-1)^2} \simeq 0.063 \ (\hat{d}=0) \tag{5.12}$$

at w_{thr} is finite, but distinctly smaller than for finite $\hat{d}$.

The value of $w_{thr}(\hat{d}=0)\simeq 3.23$ for the simplified model is larger than the solution $w_{thr}(\hat{d}=0)=2$ found for a fully flexible vesicle. Presumably, the discrepancy stems from the restricted subset of configurations in the simplified model system that is tailored for cases of strong adhesion strength w.

In any case, there are qualitative differences between the contact potential and the limit of infinitely small $\hat{d}$. For all $\hat{d}>0$, nonspherical configurations exist whose energy is lower than E_{sph} so that $w_{thr}(\hat{d}>0)\leqslant 1/2$ distinctly below $w_{thr}(\hat{d}=0)$. If $w<w_{thr}$ and $\hat{d}=0$ the vesicle unbinds, while for a wall potential of finite range $\hat{d}$ the vesicle is spherical but bound. On the other hand, as shown in Fig. 5, the curve of $\alpha(w;\hat{d}>0)$ converges pointwise towards $\alpha(w;\hat{d}=0)$.

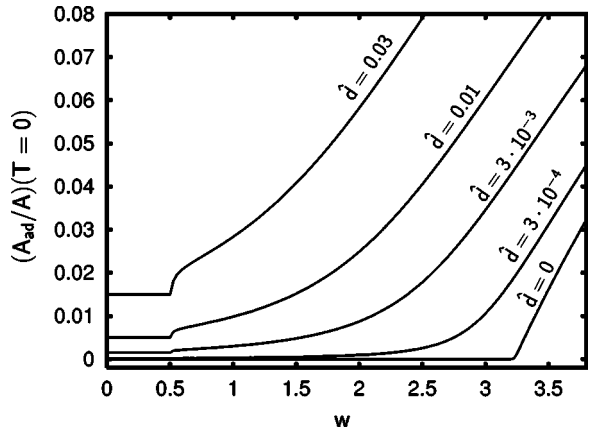

FIG. 5. The relative adhesion area $(A_{ad}/A)(w)$ of the simplified model system at $T=0$ for small w and $\hat{d}$.

The simplified model system can be used to derive an expression for $\alpha=A_{ad}/A$ as a function of the reduced potential depth w, the reduced potential range $\hat{d}$, and the reduced temperature $\hat{T}$. We start with the most simple case, which is $\hat{d}=0$ and $\hat{T}=0$. The model system is exact for large w, where $c\simeq 1$. A simple expression for

$$\alpha_0(w) \equiv \alpha(w;\hat{d}=0,\hat{T}=0) \tag{5.13}$$

results from a Taylor expansion of Eqs. (A11)–(A23) up to the third order of $w^{-1/2}$ and $(1-c)^{1/2}$. Neglecting terms of higher order, one obtains

$$\alpha_0(w) \simeq \frac{1}{2} - \frac{\pi}{4\sqrt{w}} + \frac{\pi^2-20}{16w} - \frac{\pi(\pi^2+152)}{128w^{3/2}}. \tag{5.14}$$

The expression coincides roughly with the relative adhesion area of an adhering pancakelike vesicle that consists of two flat disklike areas combined by a torus of radius $R/\sqrt{2w}$. For $w>60$, Eq. (5.14) deviates less than 1% from the exact solution, but for $w<20$ the discrepancy is already larger than 13% and grows strongly with decreasing w. Adding the next higher term from the Taylor expansion does not improve the accuracy very much. Instead, one can use the ansatz

$$\alpha_0^{(n)}(w) = 1/2 + \sum_{i=1}^{n} C_i w^{-i/2} \tag{5.15}$$

and obtain the coefficients C_i by fitting the exact solution. For $n=4$, a function

$$\alpha_0^{(4)}(w) = 1/2 - 0.73w^{-1/2} - 1.93w^{-1} + 4.97w^{-3/2} - 3.71w^{-2} \tag{5.16}$$

is found to deviate less than 0.5% from the exact solution for all w. In the following, the simple expression

$$\alpha_0(w) \equiv \frac{1}{2} - \frac{C}{\sqrt{w}} \tag{5.17}$$

with $C=0.947$ is used which already deviates less than 2% from the exact solution for all $w\geqslant 6$.

The next step is to consider $\hat{d}>0$. For a given w, the value of $\alpha(w)$ increases with increasing $\hat{d}$. For very high w, however, $\alpha(w)$ will only be slightly larger than $1/2$ as long as $\hat{d}\ll 1$. With the results shown in Fig. 3, one finds that the relative adhesion area $\alpha(w,\hat{d})$ at finite $\hat{d}$ and strong enough w can be approximated by the adhesion area $\alpha_0(w_d)$ for a vesicle adhering to a contact potential with an effective potential $w_d(w,\hat{d})$. For small adhesion strengths w the approach does not work, because $\alpha_0(w_d)$ is proportional to w, while $\alpha\geqslant\hat{d}/2$ independent of w. A good description of $\alpha(w,\hat{d})$ over the whole range of w is given by

$$\alpha(w,\hat{d}) \simeq \alpha_0(w_d) + \frac{\hat{d}}{2}. \tag{5.18}$$

The effective adhesion strength

$$w_d \equiv w(1 + c_d\sqrt{\hat{d}}) \tag{5.19}$$

with $c_d=3.0$ produces a good fit of the data. Using Eq. (5.17), one has

$$\alpha(w,\hat{d}) \simeq \frac{1+\hat{d}}{2} - \frac{0.947}{\sqrt{w(1+3.0\sqrt{\hat{d}})}}, \tag{5.20}$$

which fits the extrapolated simulation points, shown in Fig. 3 for all $w\geqslant 4.8$ with a discrepancy smaller than 3%. The deviation from the simplified model results is smaller than 5% for all $4\leqslant w<60$ and $0\leqslant\hat{d}\leqslant 0.09$. In the next section, the adhesion behavior at finite temperature is discussed.

VI. ADHESION BEHAVIOR AT FINITE TEMPERATURE

From the simulation results, it follows that for low $\hat{T}$ the reduced adhesion area α is a linear function of $\hat{T}$. The good correspondence of the extrapolated values and the analytic results for $\hat{T}=0$ indicates that the slope is indeed constant up to $\hat{T}=0$. In this section, we discuss how a constant, finite, negative slope of $\alpha(\hat{T})$ may arise from thermal fluctuations. The outcome is used to derive a function which describes all simulation results rather well.

We assume that the fluctuations of an adhering vesicle are composed of a finite number of fluctuation modes determined by a set $\underline{\xi}=(\xi_1,\ldots,\xi_k)$ of degrees of freedom ξ_i. The potential energy

$$E(\underline{\xi}) \equiv E_{el} + E_{ad} - E_0 \tag{6.1}$$

is taken as a function of $\underline{\xi}$ which has a minimum at $\underline{\xi}=\underline{0}$ with $\nabla_{\underline{\xi}}E(\underline{0})=\underline{0}$. The constant E_0 is chosen such that $E(\underline{0})=0$. The degrees of freedom are chosen such that the second derivative of E is diagonal at $\underline{\xi}=\underline{0}$,

$$E_{ij} \equiv \frac{1}{2} \left. \frac{\partial^2 E}{\partial \xi_i \partial \xi_j} \right|_{\underline{\xi}=\underline{0}} = \frac{1}{2} \left. \frac{\partial^2 E}{\partial \xi_i^2} \right|_{\underline{\xi}=\underline{0}} \delta_{ij}. \tag{6.2}$$

We assume that the temperature is low and that $E(\underline{\xi})$ diverges fast for large fluctuations ξ_i. Then, the adhesion area $A_{ad}(\underline{\xi})$ can be approximated by

$$A_{ad}(\underline{\xi}) \simeq A_{ad}(\underline{0}) + \sum_{i=1}^{k} \frac{\partial A_{ad}}{\partial \xi_i} \xi_i + \sum_{i,j=1}^{k} (A_{ad})_{ij} \xi_i \xi_j$$

$$\text{with } (A_{ad})_{ij} \equiv \frac{1}{2} \left. \frac{\partial^2 A_{ad}}{\partial \xi_i \partial \xi_j} \right|_{\underline{\xi}=\underline{0}}. \tag{6.3}$$

With the same precision one has $E(\underline{\xi}) \simeq \Sigma_{i=1}^{k} E_{ii} \xi_i^2$ and the partition function of the system becomes

$$Z \simeq \prod_{j=1}^{k} \left(\int_{-\infty}^{\infty} d\xi_j e^{-E_{jj}\xi_j^2/T} \right). \tag{6.4}$$

For the calculation of the average adhesion area

$$\langle A_{ad} \rangle = Z^{-1} \int_{-\infty}^{\infty} d\xi_1 \cdots \int_{-\infty}^{\infty} d\xi_k A_{ad}(\underline{\xi}) e^{-E/T}, \tag{6.5}$$

all terms linear in ξ_i vanish for symmetry reasons so that

$$\langle A_{ad} \rangle \simeq A_{ad}(\underline{\xi}=\underline{0}) + Z^{-1} \sum_{i=1}^{k} \int_{-\infty}^{\infty} d\xi_i (A_{ad})_{ii} \xi_i^2 e^{-E_{ii}\xi_i^2/T} \prod_{j \neq i} \int_{-\infty}^{\infty} d\xi_j e^{-E_{jj}\xi_j^2/T}$$

$$= A_{ad}(\underline{\xi}=\underline{0}) + \frac{1}{2} \sum_{i=1}^{k} \left. \frac{\partial^2 A_{ad}}{\partial \xi_i^2} \right|_{\underline{\xi}=\underline{0}} \left(\left. \frac{\partial^2 E}{\partial \xi_i^2} \right|_{\underline{\xi}=\underline{0}} \right)^{-1} T. \tag{6.6}$$

With

$$\frac{\partial^2 E_{ad}}{\partial \xi_i^2} = -\frac{w\kappa}{R^2} \frac{\partial^2 A_{ad}}{\partial \xi_i^2} = -4\pi w \kappa \frac{\partial^2 \alpha}{\partial \xi_i^2}, \tag{6.7}$$

one obtains

$$\langle \alpha \rangle = \left\langle \frac{A_{ad}}{4\pi R^2} \right\rangle \simeq \alpha(\underline{\xi}=\underline{0}) + \frac{\hat{T}}{8\pi} \sum_{i=1}^{k} \left(\frac{(E_{el})_{ii}}{4\pi\kappa\alpha_{ii}} - w \right)^{-1}, \tag{6.8}$$

where

$$\alpha_{ii} \equiv \frac{1}{2} \frac{\partial^2 \alpha}{\partial \xi_i^2}. \tag{6.9}$$

In this way, we have obtained a linear relation between α and T. If the system has k fluctuation modes that roughly contribute equally to the temperature dependence of α, one has

$$\frac{d\langle \alpha \rangle}{d\hat{T}} \simeq \frac{k}{8\pi} \left[\frac{1}{4\pi\kappa} \frac{d^2 E_{el}}{d\xi^2} \left(\frac{d^2 \alpha}{d\xi^2} \right)^{-1} - w \right]^{-1}. \tag{6.10}$$

From Eq. (6.10) it follows that $(d\langle\alpha\rangle/d\hat{T})^{-1}$ is a linear function in w. In Fig. 6, the simulation results of $(d\alpha/d\hat{T})^{-1}$ for low $\hat{T}$ are shown as a function of w. Indeed, the plots are fairly linear.

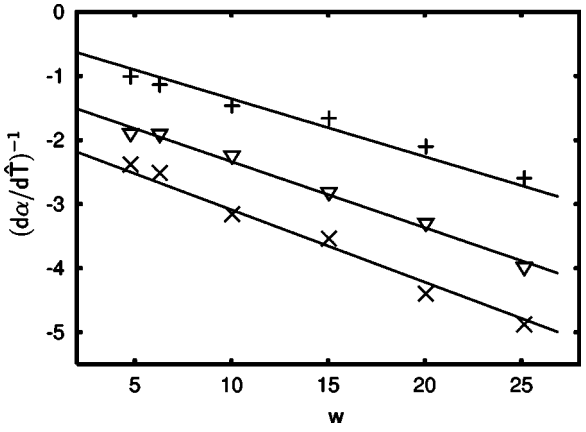

FIG. 6. The inverse slope of $\alpha(\hat{T}) = (A_{ad}/A)(\hat{T})$ as a function of w. The symbols represent simulation results for $\hat{d}=0.03$ (+), $\hat{d}=0.06$ (○), and $\hat{d}=0.09$ (▽). The straight lines are obtained from Eq. (6.13) for the respective values of $\hat{d}$.

Replacing w in Eq. (6.10) by the effective adhesion strength w_d provides the ansatz

$$\alpha(w, \hat{d}, \hat{T}) \simeq \alpha_0(w_d) + \frac{k}{8\pi} \frac{\hat{T}}{f(\hat{d}) - w_d} \tag{6.11}$$

with $\alpha_0(w_d)$ from Eq. (5.18) and a suitable function $f(\hat{d})$ that does not depend on w. With Eq. (5.18) for $\alpha_0(w_d)$ and the ansatz $f_1(\hat{d}) = c_1 + c_2\sqrt{\hat{d}}$, a least-squares fit was applied to the inverse slope of $\alpha(\hat{T})$,

$$\left(\frac{d\alpha}{d\hat{T}} \right)^{-1} = \frac{8\pi}{k} (c_1 + c_2\sqrt{\hat{d}} - w_d), \tag{6.12}$$

which revealed the fit coefficients $c_1 \simeq 27$, $c_2 \simeq -200$, and $k \simeq 423$. The results are presented in Fig. 6. Interestingly, the fit value $k=423$ for the number of fluctuation modes is roughly of the same order as the degrees of freedom of the discretized vesicle.

Altogether, one has

$$\alpha(w, \hat{d}, \hat{T}) \simeq \frac{1+\hat{d}}{2} - \frac{0.947}{\sqrt{w_d}} + \frac{423}{8\pi} \frac{\hat{T}}{27 - 200\sqrt{\hat{d}} - w_d} \tag{6.13}$$

with $w_d = w(1 + 3.0\sqrt{\hat{d}})$. In Fig. 7, the simulation results for $\alpha(T)$ are compared with Eq. (6.13). Most data points with $\alpha > 0.1$ and $\hat{T} < 0.2$ are reproduced with a deviation less than 5%, which is quite respectable: On the one hand, the range of temperatures and adhesion strengths, covered by the simulations, is quite large. On the other hand, Eq. (6.13) is simple enough to be easily transformed, a fact which is used in the following section to develop a new method to measure κ and W.

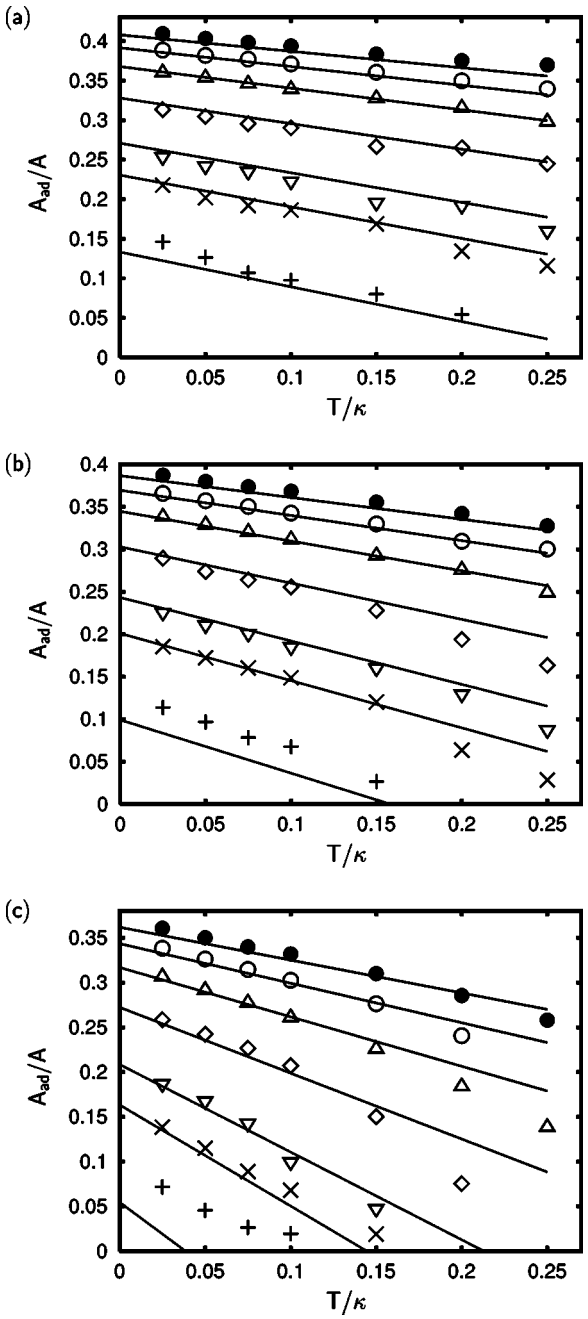

FIG. 7. Comparison of the fitting function Eq. (6.13) and the simulation data of $(A_{ad}/A)(\hat{T})$ for potential ranges (a) $\hat{d}=0.09$, (b) $\hat{d}=0.06$, (c) $\hat{d}=0.03$. The data points are simulation results for $w=2.8$ (+), $w=4.8$ (×), $w=6.3$ (▽), $w=10.0$ (◇), $w=15.0$ (△), $w=20.0$ (○), and $w=25.0$ (●). The straight lines stem from Eq. (6.13).

VII. MEASURING ADHESION STRENGTH AND BENDING RIGIDITY

Equation (6.13) provides the relative adhesion area for values of T, R, and d if κ and W are known. In practice, one is frequently confronted with the inverse problem: While the adhesion area A_{ad} can be measured, the values of W and κ are often unknown. They can be obtained by using the observed linear behavior of $\alpha(\hat{T})$ and $(d\alpha/d\hat{T})^{-1}(w)$. From Eq. (5.18), it follows that

$$WR^2 \simeq \frac{4\kappa}{1+3.0\sqrt{\hat{d}}}\left(\frac{0.947}{1+\hat{d}-2\alpha_0}\right)^2. \tag{7.1}$$

In order to use Eq. (7.1), one needs to know α_0. The observed linear behavior of $\alpha(\hat{T})$ gives

$$\alpha_0 \simeq \alpha(\hat{T}) - \frac{d\alpha(\hat{T})}{d\hat{T}}\hat{T} \tag{7.2}$$

so that, in principle, α_0 and W can be obtained by measuring $\alpha(\hat{T})$ and $d\alpha/d\hat{T}$ for finite $\hat{T}$. In practice, two difficulties may occur: (i) the values of d and κ may be unknown, and (ii) κ and R may vary with T. If κ and R depend on the temperature, Eqs. (6.13) and (7.2) are still valid, but A_{ad} is not necessarily a linear function in T. If the potential range d is known with a precision Δd, the error range ΔW of W taken from Eq. (7.1) is approximately $|\Delta W/W| \simeq \frac{3}{2}\sqrt{\hat{d}}|\Delta d/d|$. A value for $R=\sqrt{A/4\pi}$ can be determined from the unbound vesicle or a side view of the adhering vesicle. A measurement of the temperature dependence of R may be more difficult, even in cases where $(A_{ad})' \equiv dA_{ad}/dT$ can be obtained with sufficient accuracy. Further, in most cases little is known about $\kappa' \equiv d\kappa/dT$.

Nevertheless, W and κ can both be estimated from a measurement of A_{ad} and $(A_{ad})'$, if the absolute values of κ' and $R' \equiv dR/dT$ can at least be estimated to be small. In this case, one can express $d\alpha/d\hat{T}$ in Eq. (7.1) in terms of A'_{ad}, T, κ, and other terms that directly depend on T, which gives

$$\alpha_0 \simeq \alpha(T)\left(1+2T\frac{R'}{R}\right) - T\frac{(A_{ad})'}{A}\left(1+T\frac{\kappa'}{\kappa}\right). \tag{7.3}$$

If upper bounds of $|\kappa'|$ and $|R'|$ are known, Eq. (7.3) allows us to estimate the accuracy of the ansatz $\alpha_0 \simeq \alpha(T) - T(A_{ad})'/A$.

Finally, replacing all dimensionless units in Eq. (6.12) gives

$$WR^2\left(1+3.0\sqrt{\frac{d}{R}}\right) \simeq \kappa\left(27-200\sqrt{\frac{d}{R}}\right) - \frac{423}{8\pi}\frac{A}{(A_{ad})'} \times\left(1-T\frac{\kappa'}{\kappa}+2\frac{A_{ad}}{(A_{ad})'}\frac{R'}{R}\right). \tag{7.4}$$

With Eqs. (7.1)–(7.4), the quantities $W(T)$ and $\kappa(T)$ can be estimated by measuring $\alpha(T)$ and $\alpha(T\pm\Delta T)$. As a consistency check of the assumption that κ' and R' are small, one should prove the linearity of $A_{ad}(T)$.

VIII. CONCLUSIONS

With the help of Monte Carlo simulations, we have investigated the temperature dependence of the adhesion of fluid vesicles in the absence of an osmotic pressure. For temperatures $\hat{T}<0.2$, the relative adhesion area $\alpha(\hat{T})$ is found to be a

linear function of $\hat{T}$. This result is found for a wide range of adhesion strengths w and potential widths $\hat{d}$. An expression for $\alpha(w,\hat{d},\hat{T})$ is derived that describes the adhesion behavior in the linear regime.

The expression found for $\alpha(w,\hat{d},\hat{T})$ is simple enough to be inverted such that the adhesion strength W and the bending rigidity κ can be found by measuring the adhesion area A_{ad} at different temperatures T.

The linear behavior of $\alpha(\hat{T})$ is described by an analytic approach, which considers contributions to $d\alpha/d\hat{T}$ by a set of orthogonal fluctuation modes. The ansatz provides a finite constant slope of $\alpha(\hat{T})$ down to $\hat{T}=0$. A more quantitative estimate of the mode contributions, which requires a more complex model system than the one treated here, would be of great interest. The same is true for an investigation of the temperature dependence of α in the case of a finite pressure difference.

APPENDIX A: ENERGY EXPRESSIONS FOR THE ANALYTIC MODEL

A simplified model for an adhering vesicle at $\hat{T}=0$ is introduced in Sec. V. In the following, the energy expressions in Eqs. (5.5) and (5.6) are derived.

The model vesicle with an efficient contact angle θ_c and $c=\cos(\theta_c)$ has a circular base area of the size

$$A_{ba} = \pi R_{ba}^2, \tag{A1}$$

a spherical cap area

$$A_{sc} = \int_0^{2\pi} d\varphi \int_0^{\theta_c} d\theta R_{sc}^2 \sin(\theta) = 2\pi(1-c)R_{sc}^2, \tag{A2}$$

and a torus segment which can be parametrized as

$$\underline{r}(\theta,\varphi) = \begin{pmatrix} [R_{ba} + R_{co}\sin(\theta)]\cos(\varphi) \\ [R_{ba} + R_{co}\sin(\theta)]\sin(\varphi) \\ R_{co}[\cos(\theta)+1] \end{pmatrix}$$
$$\text{with } \varphi \in [0,2\pi) \text{ and } \theta \in [\theta_c,\pi). \tag{A3}$$

With the determinant

$$g = R_{co}^2[R_{ba} + R_{co}\sin(\theta)]^2 \tag{A4}$$

of the metric tensor $g_{ij}=D_i\underline{r}\cdot D_j\underline{r}$, the area of the torus segment becomes

$$A_{co} = \int_0^{2\pi} d\varphi \int_{\theta_c}^{\pi} d\theta\sqrt{g}$$
$$= 2\pi R_{co}[R_{ba}\arccos(-c) + R_{co}(1+c)]. \tag{A5}$$

At $\theta=\theta_c$, the spherical cap and the torus segment must match,

$$R_{sc}\sqrt{1-c^2} = R_{ba} + R_{co}\sqrt{1-c^2}. \tag{A6}$$

With

$$\lambda \equiv R_{ba}/R_{co}, \tag{A7}$$

the total vesicle area becomes

$$A = A_{ba} + A_{sc} + A_{co}$$
$$= \pi R_{co}^2\left[\lambda^2 + \frac{2(\lambda+\sqrt{1-c^2})^2}{1+c} + 2\lambda\arccos(-c) + 2(1+c)\right]. \tag{A8}$$

On the other hand, from Eq. (5.1) it follows that

$$A = 4\pi R^2 = 8\pi R_{co}^2 w. \tag{A9}$$

Equating Eqs. (A8) and (A9) gives a quadratic equation in λ,

$$8w(1+c) = (3+c)\lambda^2 + 2[2\sqrt{1-c^2} + (1+c)\arccos(-c)]\lambda + 4(1+c). \tag{A10}$$

It follows that

$$\lambda = \sqrt{u^2(c) + \frac{4(1+c)(2w-1)}{3+c}} - u(c)$$
$$\text{with } u(c) \equiv \frac{2\sqrt{1-c^2} + (1+c)\arccos(-c)}{3+c}. \tag{A11}$$

The energy $E=E_{ad}+E_{el}$ of the system is the sum of the adhesion energy E_{ad} and the elastic curvature energy E_{el}.

The elastic curvature energy includes contributions from the spherical cap E_{el}^{sc},

$$E_{el}^{sc} = \frac{\kappa}{2}\int_0^{2\pi} d\varphi \int_0^{\theta_c} d\theta (2H)^2\sqrt{g}$$
$$= \pi\kappa(1-c)R_{sc}^2\left(\frac{2}{R_{sc}}\right)^2 = 4\pi\kappa(1-c) \tag{A12}$$

and the torus segment E_{el}^{co},

$$E_{el}^{co} = \frac{\kappa}{2}\int_0^{2\pi} d\varphi \int_{\theta_c}^{\pi} d\theta (2H)^2\sqrt{g} \tag{A13}$$

$$= \kappa\pi\int_{\theta_c}^{\pi} d\theta\left(2\frac{R_{ba}+2R_{co}\sin(\theta)}{2R_{ba}R_{co}+2R_{co}^2\sin(\theta)}\right)^2 \times R_{co}[R_{ba}+R_{co}\sin(\theta_c)] \tag{A14}$$

$$= \kappa\pi\int_{\theta_c}^{\pi} d\theta\frac{[\lambda+2\sin(\theta)]^2}{\lambda+\sin(\theta)}. \tag{A15}$$

Depending on the value of λ, one has

$$E_{el} = 8\pi\kappa + 2\pi\kappa\frac{\lambda^2}{\sqrt{\lambda^2-1}}\arctan\left(\frac{(1+c)\sqrt{\lambda^2-1}}{(1+c)+\lambda\sqrt{1-c^2}}\right)$$
$$\text{for } \lambda > 1,$$

$$= 8\pi\kappa + \pi\kappa\left(1+\frac{c}{1+\sqrt{1-c^2}}\right) \quad \text{for } \lambda = 1, \tag{A16}$$

$$= 8\pi\kappa + \pi\kappa \frac{\lambda^2}{\sqrt{1-\lambda^2}} \times \log\left(\frac{(1+c)(1+\sqrt{1-\lambda^2}) + \lambda\sqrt{1-c^2}}{(1+c)(1-\sqrt{1-\lambda^2}) + \lambda\sqrt{1-c^2}} \right) \quad \text{for } \lambda < 1.$$

The adhesion energy $E_{ad} = -WA_{ad}$ is proportional to the size of the adhesion area A_{ad}. For $\hat{d} = 0$, the adhesion area A_{ad} coincides with the circular base area A_{ba},

$$E_{ad}^{ba} = -\frac{w\kappa}{R^2}\pi R_{ba}^2 = -\frac{\kappa\pi}{2}\lambda^2. \tag{A17}$$

For $\hat{d} > 0$, also the torus segment contributes to A_{ad}. If the adhesion range d is smaller than the height $R_{co}[\cos(\theta_c) + 1]$ of the torus segment, the total adhesion energy is given by $E_{ad} = E_{ad}^{ba} + E_{ad}^{co}(\theta_{co})$, where

$$E_{ad}^{co}(\theta_{co}) = -\frac{w\kappa}{R^2}\int_0^{2\pi} d\varphi \int_{\theta_{co}}^{\pi} d\theta \sqrt{g} = -\pi\kappa\{\lambda \arccos[-\cos(\theta_{co})] + [1 + \cos(\theta_{co})]\} \tag{A18}$$

and θ_{co} is determined by the potential range via $\cos(\theta_{co}) = (d/R_{co}) - 1 = \hat{d}\sqrt{2w} - 1$. If d is larger than the height of the torus segment so that $\hat{d}\sqrt{2w} > 1 + c$, the total adhesion energy is given by $E_{ad} = E_{ad}^{ba} + E_{ad}^{co}(\theta_c) + E_{ad}^{sc}(\theta_{sc})$, where $E_{ad}^{sc}(\theta_{sc})$ represents the adhered part of the spherical cap,

$$E_{ad}^{sc}(\theta_{sc}) = -\frac{w\kappa}{R^2}\int_0^{2\pi} d\varphi \int_{\theta_{sc}}^{\theta_c} d\theta R_{sc}^2 \sin(\theta) = -\frac{2\pi w\kappa}{R^2} R_{sc}^2[\cos(\theta_{sc}) - \cos(\theta_c)]. \tag{A19}$$

Here, θ_{sc} corresponds to the upper edge of the adhesion area,

$$R_{sc}[\cos(\theta_{sc}) - \cos(\theta_c)] + R_{co}[\cos(\theta_c) + 1] = d \tag{A20}$$

so that

$$E_{ad}^{sc} = -\pi\kappa \frac{R_{sc}}{R_{co}}\left(\frac{d}{R_{co}} - (1 + c) \right). \tag{A21}$$

Altogether, one has

$$E_{ad} = -\pi\kappa\left[\frac{1}{2}\lambda^2 + \lambda \arccos(1 - \hat{d}\sqrt{2w}) + \hat{d}\sqrt{2w} \right] \quad \text{for } \hat{d}\sqrt{2w} \leq 1 + c \tag{A22}$$

and

$$E_{ad} = -\pi\kappa\left[\frac{1}{2}\lambda^2 + \lambda \arccos[1 - (1 + c)] + (1 + c) + \left(\frac{\lambda}{\sqrt{1-c^2}} + 1 \right)[\hat{d}\sqrt{2w} - (1 + c)] \right] \quad \text{for } \hat{d}\sqrt{2w} > 1 + c. \tag{A23}$$

Using $m = \min\{\hat{d}\sqrt{2w}, 1 + c\}$, the adhesion energy can be written in the closed expression given in Eq. (5.5).

[1] D. P. Nikolelis and S. Pantoulias, Biosens. Bioelectron. **15**, 439 (2000).
[2] M. I. Fisher and T. Tjärnhage, Biosens. Bioelectron. **15**, 463 (2000).
[3] B. J. Chang *et al.*, Colloids Surf., A **198**, 519 (2002).
[4] A. Raudino, A. Cambria, M. P. Sarpietro, and Christina Satriano, J. Colloid Interface Sci. **231**, 66 (2000).
[5] *Handbook of Biological Physics*, edited by R. Lipowsky and E. Sackmann (Elsevier, Amsterdam, 1995).
[6] *Vesicles*, edited by M. Rosoff (Marcel Dekker, New York, 1996).
[7] J. O. Rädler, T. J. Feder, H. H. Strey, and E. Sackmann, Phys. Rev. A **51**, 4526 (1995).
[8] N. Fang, V. Chan, K.-T. Wan, H.-Q. Mao, and K. W. Leong, Colloids Surf., B **25**, 347 (2002).
[9] A.-L. Bernard, M.-A. Guedeau-Boudeville, L. Jullien, and J.-M. di Meglio, Europhys. Lett. **46**, 101 (1999).
[10] S. Sofou and J. L. Thomas, Biosens. Bioelectron. **18**, 445 (2003).
[11] F. Tokumasu, F. J. Jin, G. W. Feigenson, and J. A. Dvorak, Ultramicroscopy **97**, 217 (2003).
[12] S. M. Bailey, S. Chiruvolu, J. Israelachvili, and J. A. N. Zasadzinski, Langmuir **6**, 1326 (1990).
[13] S. W. Hui, T. P. Stewart, L. T. Boni, and P. L. Yeagle, Science **212**, 921 (1981).
[14] L. Miao, U. Seifert, M. Wortis, and H.-G. Döbereiner, Phys. Rev. E **49**, 5389 (1994).
[15] H.-G. Döbereiner, G. Gompper, C. Haluska, D. M. Kroll, P. G. Petrov, and K. A. Riske, Phys. Rev. Lett. **91**, 048301 (2003).
[16] H. P. Duwe, J. Käs, and E. Sackmann, J. Phys. (France) **51**, 945 (1990).
[17] U. Seifert and R. Lipowsky, Phys. Rev. A **42**, 4768 (1990).
[18] R. Lipowsky and U. Seifert, Langmuir **7**, 1867 (1991).
[19] R. Lipowsky and U. Seifert, Mol. Cryst. Liq. Cryst. **202**, 17 (1991).
[20] W. Helfrich, Z. Naturforsch. C **28c**, 693 (1973).
[21] G. Gompper and D. M. Kroll, J. Phys.: Condens. Matter **9**, 8795 (1997).
[22] F. Jülicher, Ph.D. thesis, University of Cologne (1993); J. Phys. II **6**, 1797 (1996).